

## Oxidation of $\text{Al}_2\text{O}_3$ -dispersion chromizing coating by pack-cementation at 800 °C

ZHOU Yue-bo(周月波), CHEN Hong-yu(陈洪玉), ZHANG Hai-jun(张海军), WANG Yong-dong(王永东)

College of Materials Science and Engineering, Heilongjiang Institute of Science and Technology,  
Harbin 150027, China

Received 22 June 2007; accepted 13 November 2007

**Abstract:** Preparation and oxidation of an  $\text{Al}_2\text{O}_3$ -dispersed chromizing coating were investigated by chromizing an as-electrodeposited Ni- $\text{Al}_2\text{O}_3$  nanocomposite film using a conventional pack-cementation method at a greatly decreased temperature (800 °C). For comparison, chromizing was also performed with the same condition on an as-deposited Ni film without  $\text{Al}_2\text{O}_3$  nanoparticles. Oxidation at 900 °C indicates that, compared with the  $\text{Al}_2\text{O}_3$ -free chromizing coating, the  $\text{Al}_2\text{O}_3$ -dispersed chromizing coating exhibits a increased oxidation resistance, due to the formation of purer and denser chromia scale. The effect of  $\text{Al}_2\text{O}_3$  on the coating formation and the coating oxidation behavior was discussed in details.

**Key words:** electrodeposition; composite coating; oxidation; reactive element effect

### 1 Introduction

Chromizing is one of the widely used surface coating technologies to economically improve high temperature oxidation and corrosion resistance of components[1–2]. Various chromizing processes have been developed, such as the pack cementation method, the molten-salt technique, and the vacuum chromizing process. Pack-cementation is one of the easiest and cheapest processes to obtain the chromizing coatings. Unfortunately, the pack-cementation was normally performed at temperatures above 1 000 °C, limited by the diffusion and reaction kinetics involved. Such a high temperature treatment inevitably limits the applications of chromizing coatings due to grain growth of the substrate materials, which has a detrimental effect on the mechanical properties of workpieces. Therefore, reducing pack-cementation temperature is required for widespread application of the chromizing coatings. Recently, a novel chromizing[3–5]/alumizing[6–7] technique at low temperature on nano-structured coatings produced using so-called surface mechanical attrition treatment (SMAT) was developed. The results exhibited that after the same treatment, much thicker Cr/Al-diffusion layers were obtained in the SMAT sample than

in the coarse-grained one due to a large volume fraction of grain boundaries promoting the diffusion of Cr/Al. Compared with SMAT, electrodeposition is another method to produce nanostructured materials, and seems to be appropriate for lowering the chromizing temperature in a practical manner. At the same time, the grain of the chromizing coating would be further optimized by the co-deposition of inert oxide particles. The effects of added oxide on the chromization may be summarized as follows[8]: 1) retarding the grain growth of the chromizing coating at high temperature by anchoring the movement of grain boundaries; and 2) producing numerous metal/oxide interphase boundaries, which would be additional short-circuit paths in addition to grain boundaries for chromium transport. The refinement of grain of the chromizing coating would enhance Cr diffusion to the oxidation front and consequently accelerate the formation of a continuous chromia scale. Reactive element oxides are, of course, such desired inert oxide particles. Besides, once being introduced into the inward-growth chromizing coating, they would potentially improve the oxidation resistance of the chromizing coating due to “reactive element effect (REE)”[9]. By considering the beneficial effect of RE oxides on oxidation,  $\text{CeO}_2$  particles were added into chromium coatings by chromizing the co-deposited Ni-

$\text{CeO}_2$  nanocomposite coatings at 120 °C or 700 °C [8, 10–11]. In this contribution, by considering the same effect of  $\text{Al}_2\text{O}_3$  on the grain growth and oxidation,  $\text{Al}_2\text{O}_3$ -dispersion chromizing coating was produced at 800 °C using the same process, and its oxidation performance was reported. For comparison, preparation and oxidation of chromium coatings on the Ni film were also carried out under the same condition.

## 2 Experimental

Samples with dimensions of 15 mm×10 mm×2 mm were cut from an electrolytic nickel plate. They were ground to a final 800# SiC paper. After ultrasonic cleaning in acetone, they were electrodeposited with a 40  $\mu\text{m}$ -thick film of Ni- $\text{Al}_2\text{O}_3$  nanocomposite from a nickel sulfate bath containing certain content of  $\text{Al}_2\text{O}_3$  nanoparticles with a average particle size of 90 nm. The current density used was 3 A/dm<sup>2</sup>, the bath temperature 35 °C, and the pH 5.6–6.2. For comparison, a 50  $\mu\text{m}$ -thick Ni film was also electroplated on Ni. During the electrodeposition, the electrolyte was magnetically stirred in order to keep the particles dispersed and suspended in the electrolyte. Chromizing on the samples coated with the Ni- $\text{Al}_2\text{O}_3$  nanocomposite and nickel film was carried out using pack cementation at 800 °C for 5 h in a powder mixture of 50%Cr (particle size 75  $\mu\text{m}$ )+47% $\text{Al}_2\text{O}_3$  (particle size 75  $\mu\text{m}$ )+3% $\text{NH}_4\text{Cl}$  (in mass percentage) in pure Ar atmosphere. Afterward the chromized samples were brushed, cleaned in bubbling distilled water for 30 min and finally ultrasonically cleaned in acetone to remove any loosely embedded pack particles. The oxidation experiments were carried out in air at 900 °C up to 20 h and the mass measurements were conducted after fixed time intervals using a balance with 0.01 mg sensitivity. The microstructure of the various chromized coatings before and after oxidation was investigated using transmission electron microscopy (TEM), scanning electron microscopy (SEM) with energy dispersive X-ray analysis (EDAX), and X-ray diffractometry (XRD).

## 3 Results

### 3.1 Microstructure

Fig.1 shows the surface morphology of the as-co-deposited Ni- $\text{Al}_2\text{O}_3$  nanocomposite. Bright  $\text{Al}_2\text{O}_3$  nanoparticles were, in general, homogeneously dispersed in the nanocomposite film, although some of them formed agglomerated clusters. EDAX results showed that the as-co-deposited nanocomposite film contained

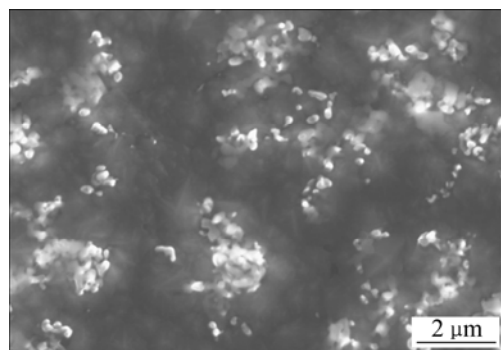


**Fig.1** Surface morphology of Ni- $\text{Al}_2\text{O}_3$  nanocomposite

around 7%–9% $\text{Al}_2\text{O}_3$ .

Parallel TEM characterization indicated that the grain sizes of Ni deposits were generally in the range of 15–60 nm, as seen in Fig.2(a). Fig.2(b) shows a bright-field TEM image, in which  $\text{Al}_2\text{O}_3$  particles were homogeneously dispersed in the nanocrystalline Ni matrix. Clearly, the Ni- $\text{Al}_2\text{O}_3$  nanocomposite had finer grain than the Ni-film. Both films formed numerous twins. No defects such as pores and cracks were seen.

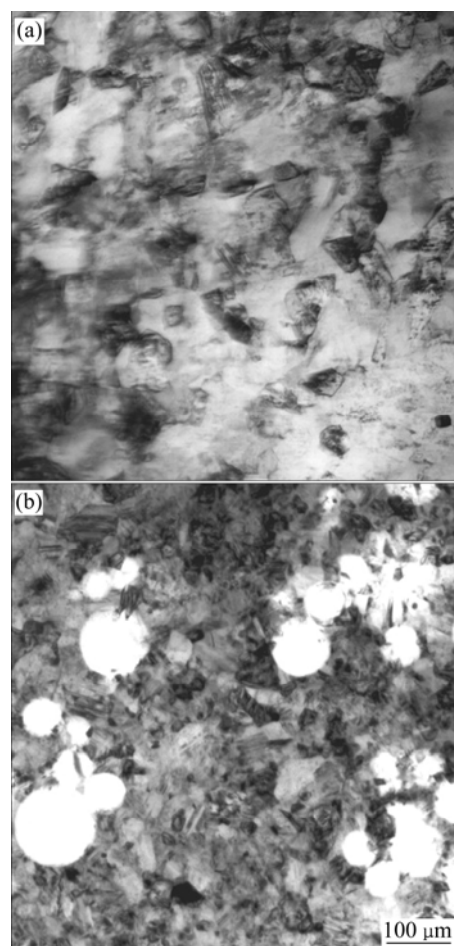


**Fig.2** TEM bright-field images of Ni-film (a) and Ni- $\text{Al}_2\text{O}_3$  nanocomposite (b)

After pack cementation, chromized layers were prepared. The chromium concentrations on the surface zone ( $<4 \mu\text{m}$ , from the profile depth of electron beam) were about 50% for the chromized Ni coating, and about 58% for the chromized Ni-Al<sub>2</sub>O<sub>3</sub> nanocomposite coating on the basis of EDAX analysis. Fig.3 shows the corresponding cross-sectional micrographs of two chromizing coatings. The chromizing coatings on Ni film exhibited a double-layer structure: relatively equiaxed grains in outer layer and columnar ones in inner layer. Here, it is noteworthy that the gray spot in the chromized Ni-Al<sub>2</sub>O<sub>3</sub> nanocomposite, indicated by arrows, are the dispersed Al<sub>2</sub>O<sub>3</sub> particles. They were from the co-deposited Al<sub>2</sub>O<sub>3</sub> nanoparticles in the composite. From Fig.3(b), it is clear that the co-deposited Al<sub>2</sub>O<sub>3</sub> particles dispersed in the whole chromizing coating. The thickness of chromized layers on Ni coating and Ni-Al<sub>2</sub>O<sub>3</sub> composite coating was about 32 and 38  $\mu\text{m}$ , respectively. TEM observations showed that the grain size of the Al<sub>2</sub>O<sub>3</sub>-free chromium coating was generally larger than 1 200 nm (Fig.4(a)). In contrast, the grain size of the Al<sub>2</sub>O<sub>3</sub>-dispersed chromium coating was generally below 700 nm (Fig.4(b)), indicating that the grain growth of the Al<sub>2</sub>O<sub>3</sub>-free chromium coating was retarded by the dispersed Al<sub>2</sub>O<sub>3</sub>. The dispersoids (as arrowed in Fig.4(b)) were the original nanoparticles used. The refinement of grain size of the chromizing coating would enhance the diffusion of chromium during pack cementation and lead to higher Cr content of the Al<sub>2</sub>O<sub>3</sub>-dispersed chromium coating than that of the Al<sub>2</sub>O<sub>3</sub>-free coating at a given distance from the coating surface, as seen in Fig.5.

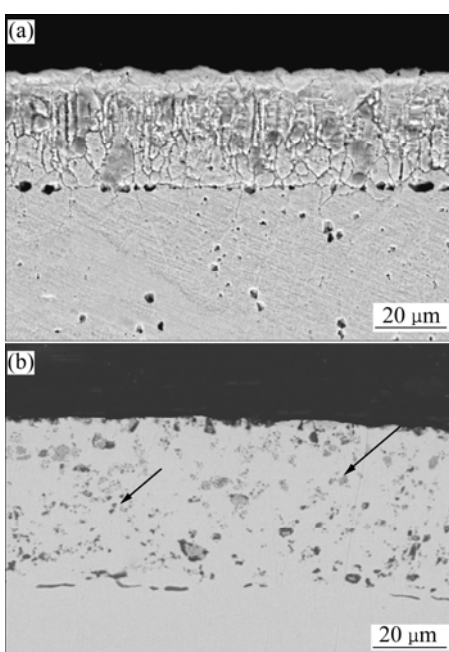


**Fig.3** Cross-sectional micrographs of chromizing coatings on Ni film (a) and Ni-Al<sub>2</sub>O<sub>3</sub> nanocomposite (b)

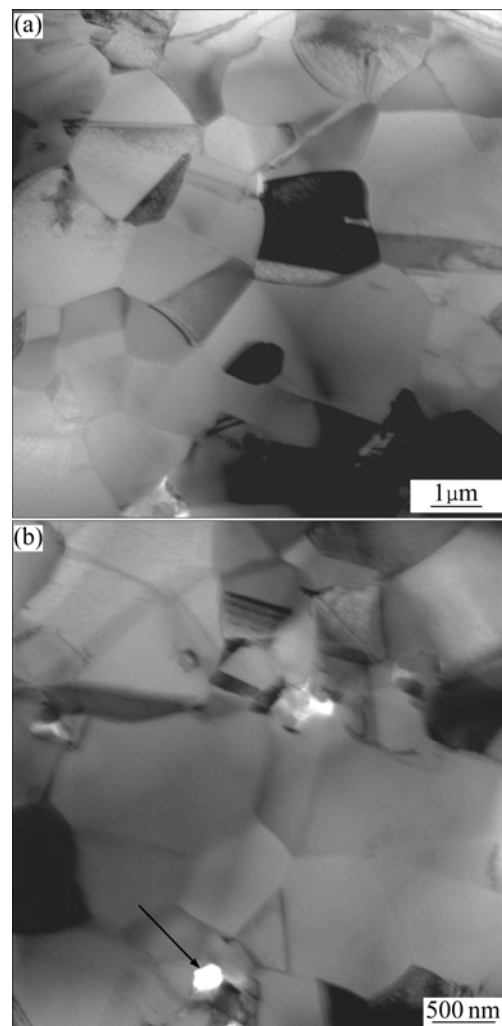


**Fig.4** TEM bright-field images of chromized coatings on Ni-film (a) and Ni-Al<sub>2</sub>O<sub>3</sub> nanocomposite (b)

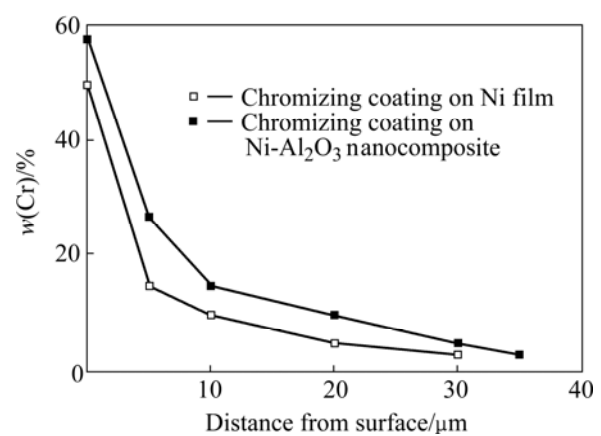


**Fig.5** Chromium concentration profiles for two chromizing coatings at 800 °C for 5 h

### 3.2 Oxidation performance

Fig.6 shows the oxidation kinetics of two chromizing coatings in air for 20 h. During oxidation and cooling, no spallation occurred for the two chromizing

coatings. Clearly, the  $\text{Al}_2\text{O}_3$ -dispersed chromium coating exhibited an apparently low scaling rate during a short transient stage of oxidation (the first 2–3 h). After this period, the oxidation rate maintained so extremely low that no significant mass gain occurred. However, a significant mass gain occurred for the  $\text{Al}_2\text{O}_3$ -free chromium coating. Compared with the chromizing coating on the pure Ni film, the one on the Ni- $\text{Al}_2\text{O}_3$  nanocomposite coating had an apparently low scaling rate during the entire stage of oxidation.

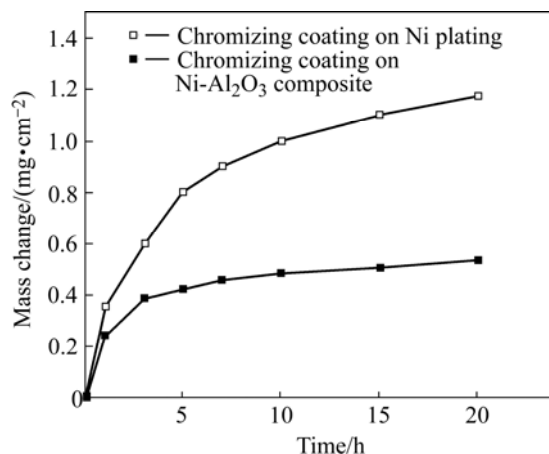


Fig.6 Oxidation kinetics of two chromizing coatings at 900 °C for 20 h

### 3.3 Scale microstructure and composition

The XRD characterization demonstrated that the oxide phases on the chromized Ni film were composed of  $\text{NiO}$ ,  $\text{NiCr}_2\text{O}_4$  and  $\text{Cr}_2\text{O}_3$ , as seen in Fig.7(a). In the meantime, the probed intensities of the peaks of  $\text{NiO}$  and  $\text{NiCr}_2\text{O}_4$  spinel were both extremely weaker than those of  $\text{Cr}_2\text{O}_3$ . However, a purer chromia scale was formed on the  $\text{Al}_2\text{O}_3$ -dispersed chromium coating, as seen in Fig.7(b). This suggested that the  $\text{Al}_2\text{O}_3$  addition significantly suppressed  $\text{NiO}$  growth, and a purer chromia

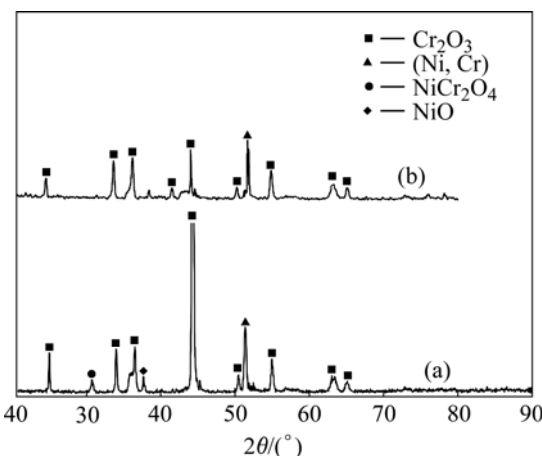


Fig.7 Comparison of XRD patterns of oxide scales formed on two chromizing coatings at 900 °C for 20 h: (a) Ni film; (b) Ni- $\text{Al}_2\text{O}_3$  nanocomposite

scale was formed on the  $\text{Al}_2\text{O}_3$ -dispersed chromium coating.

Fig.8 shows the cross-sectional micrographs of the scales formed on two chromizing coatings after exposure at 900 °C for 20 h. The chromized Ni film formed a continuous chromia layer, on which Ni-rich oxide was seen. And the scale was significantly buckled. Cracks below buckles were seen ("A" indicated in Fig.8(a)). Besides, internal oxidation of chromium occurred in some regions. In contrast, the scale formed on chromized Ni- $\text{Al}_2\text{O}_3$  nanocomposite coating was very flat and scale spallation and internal oxidation did not occur (Fig.8(b)).

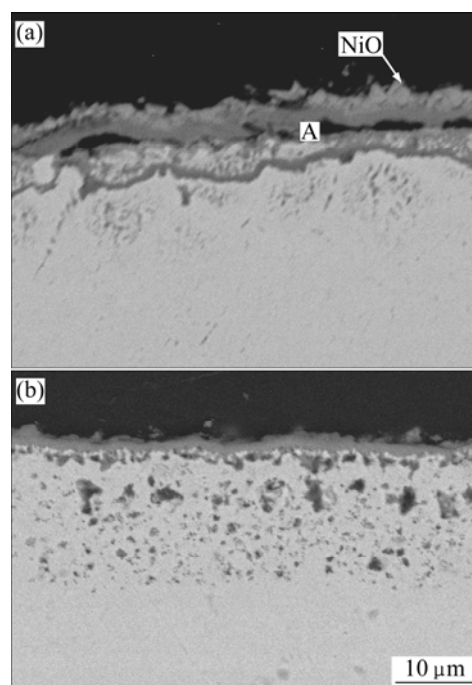


Fig.8 Cross-sectional micrographs of chromizing coatings on Ni film (a) and Ni- $\text{Al}_2\text{O}_3$  nanocomposite (b) at 900 °C in air for 20 h

## 4 Discussion

In general, all chromium coatings exhibited a double-layered structure. The outer layers formed from the contribution of the outward growth, and the inner layers formed from the contribution of the inward growth. The chromizing coating on the Ni-plated sample exhibited a very thin outer layer, implying that the outward growth also contributed to the formation of the chromizing coating for Ni film. Fig.3(b) showed that the co-deposited  $\text{Al}_2\text{O}_3$  nanoparticles homogeneously dispersed in the whole chromizing coating, implying that the chromizing processing was controlled by inward chromium diffusion. From the comparison of the grain size of the coatings with and without  $\text{Al}_2\text{O}_3$  particles before (Fig.2) and after chromizing treatment (Fig.4), it was concluded that the dispersed  $\text{Al}_2\text{O}_3$  particles

significantly retarded the grain growth of the chromizing coating during the pack cementation process. The grain refinement would enhance the diffusion of chromium during pack cementation [8, 10–11], which led to higher Cr content for Al<sub>2</sub>O<sub>3</sub>-dispersed chromizing coating than that for Al<sub>2</sub>O<sub>3</sub>-free coating at a given distance from the coating surface, as seen in Fig.5.

As compared with the oxidation of the chromium coating on the Ni-plated sample, that on the Ni-Y<sub>2</sub>O<sub>3</sub> coated sample exhibited a short-term transient oxidation period and an apparently low scaling rate (Fig.6), as a result of the formation of a purer and denser chromia scale, as seen in Figs.7 and 8. From Fig.6, it could be also seen that the Al<sub>2</sub>O<sub>3</sub>-dispersed chromizing coating exhibited an apparently low scaling rate, particularly in the initial stage. The reason can be interpreted as follows. The increased grain boundaries due to the grain refinement of the chromizing coating for the Al<sub>2</sub>O<sub>3</sub>-dispersed chromizing coating, together with dispersed Al<sub>2</sub>O<sub>3</sub> particles on the coating surface, are both available sites for chromia nucleation at onset of oxidation. The increased chromia nuclei shorten the time for their linkage through the oxide lateral growth. Furthermore, the lateral growth can be enhanced by accelerated chromium diffusion to the oxidation front via the increased grain boundaries in the finer-grained coating [8,10–14].

By comparison of the cross sectional morphologies of the scales formed on the chromizing coatings with and without Al<sub>2</sub>O<sub>3</sub> in Fig.6, cavities below the scales formed on the chromized nickel-coating. They formed as a result of condensation of chromium cation vacancies at the interface, which were injected from the scale counter balancing the outward chromium diffusion during oxidation, or from the coating substrate resulting from the relative diffusion rate of Ni to Cr into the coating interior due to the Kirkendall effect. The reason lies that a low consumption rate of chromium by oxidation due to the formation of purer and denser chromia scale on the Al<sub>2</sub>O<sub>3</sub>-dispersed chromizing coating reduces the flux of the cation vacancies toward the interface and retards the formation of interfacial cavities below the scales. Moreover, the added Al<sub>2</sub>O<sub>3</sub> may have a “REE” as reactive element to decrease the formation of interfacial cavities through an inversion of chromia growth mechanisms from predominant outward cation diffusion in the absence of RE into dominant inward oxygen diffusion [12–16], which needs further investigation.

## 5 Conclusions

1) By pack cementation on the as-electrodeposited Ni-Al<sub>2</sub>O<sub>3</sub> nanocomposite at 800 °C, an Al<sub>2</sub>O<sub>3</sub>-dispersed chromizing coatings were manufactured.

2) At low temperature, the chromizing processing was controlled by inward chromium diffusion for Ni-Al<sub>2</sub>O<sub>3</sub> nanocomposite film. However the outward growth also contributed to the formation of the chromizing coating for Ni film.

3) The co-deposited Al<sub>2</sub>O<sub>3</sub> nanoparticles significantly retarded the grain growth of the chromizing coatings by anchoring the movement of grain boundaries, which enhanced Cr diffusion to the oxidation front and consequently accelerated the formation of a continuous pure chromia scale in a short transient stage of oxidation.

## References

- [1] LEE J W, DUH J G, TSAI S Y. Corrosion resistance and microstructural evaluation of the chromized coating process in a dual phase Fe-Mn-Al-Cr alloy [J]. Surf Coat Technol, 2002, 153: 59–66.
- [2] MEIER G H, CHENG C, PERKINS R A, BAKKER W. Diffusion chromizing of ferrous alloys [J]. Surf Coat Technol, 1989, 39/40: 53–64.
- [3] WANG Z B, TAO N R, TONG W P, LU J, LU K. Diffusion of chromium in nanocrystalline iron produced by means of surface mechanical attrition treatment [J]. Acta Mater, 2003, 51: 4319–4329.
- [4] WANG Z B, LU J, LU K. Chromizing behaviors of a low carbon steel processed by means of surface mechanical attrition treatment [J]. Acta Materialia, 2005, 53: 2081–2089.
- [5] WANG Z B, LU J, LU K. Wear and corrosion properties of a low carbon steel processed by means of SMAT followed by lower temperature chromizing treatment [J]. Surf Coat Technol, 2006, 201: 2796–2801.
- [6] ZHAN Zhao-lin, HE Ye-dong, WANG De-ren, GAO Wei. Preparation of aluminide coatings at relatively low temperature [J]. Trans Nonferrous Met Soc China, 2006, 16(3): 647–653.
- [7] ZHAN Zhao-lin, HE Ye-dong, WANG De-ren, GAO Wei. Aluminide coatings formed on Fe-13Cr steel at low temperature and its oxidation resistance[J]. Oxidation of Metals, 2007, 68(5/6): 243–251
- [8] ZHANG H, PENG X, ZHAO J, WANG F. Prior electrodeposition of nanocrystalline Ni-CeO<sub>2</sub> film fabricating an oxidation resistant chromized coating on carbon steels [J]. Electrochemical and Solid-state Letters, 2007, 10(3): C12–C15.
- [9] PFEIL B. Improvement in heat-resisting alloys UK Patent, 459848[P]. 1937.
- [10] ZHU L, PENG X, YAN J, WANG F. Oxidation of a novel chromium coating with CeO<sub>2</sub> dispersions[J]. Oxid Met, 2004, 62: 411–426.
- [11] YAN J, PENG X, WANG F. Oxidation of a novel CeO<sub>2</sub>-dispersion-strengthened chromium coating in simulated coal-combustion gases [J]. Mater Sci and Eng A, 2006, 426: 266–273.
- [12] MOON D P. Role of reactive elements in alloy protection [J]. Mater Sci Technol, 1989, 5: 754–763.
- [13] HOU P Y, STRINGER J. The effect of reactive element additions on the selective oxidation, growth and adhesion of chromia scales [J]. Mater Sci and Eng A, 1995, 202: 1–10.
- [14] HOU P Y, STRINGER J. The influence of ion-implanted yttrium on the selective oxidation of chromium in Co-25%Cr [J]. Oxid Met, 1988, 29: 45–73.
- [15] YUREK G J, PRZYBYLSKI K, GARRATT-REED A J. Segregation of Y to grain boundaries in Cr<sub>2</sub>O<sub>3</sub> and NiO scales formed on an ODS alloy [J]. J Electrochem Soc, 1987, 134: 2643–2644.
- [16] COTELL C M, YUREK G J, HUSSEY R J, MITCHELL D F, GRAHAM M J. The influence of grain-boundary segregation of Y in Cr<sub>2</sub>O<sub>3</sub> on the oxidation of Cr metal [J]. Oxid Met, 1990, 34: 173–200.

(Edited by YANG Bing)